



Available online at www.sciencedirect.com

ScienceDirect



Nuclear Physics A 982 (2019) 8-14

www.elsevier.com/locate/nuclphysa

XXVIIth International Conference on Ultrarelativistic Nucleus-Nucleus Collisions (Quark Matter 2018)

Highlights from the ATLAS experiment

Iwona Grabowska-Bold on behalf of the ATLAS Collaboration^a,

^aAGH University of Science and Technology, Kraków, Poland

Abstract

This report provides an overview of the new results obtained by the ATLAS Collaboration at the LHC, which were presented at the Quark Matter 2018 conference. These measurements were covered in 12 parallel talks, one flash talk and 11 posters. In this document, a discussion of results is grouped into four areas: electromagnetic interactions, jet quenching, quarkonia and heavy-flavour production, and collectivity in small and larger systems. Measurements from the xenon-xenon collisions based on a short run collected in October 2017 are reported for the first time.

Keywords: ATLAS experiment, quark-gluon plasma, photon-induced processes, jet quenching, quarkonia production, heavy-flavour production, collectivity in small systems, xenon-xenon collisions

1. Introduction

In addition to proton-proton (pp) physics, the ATLAS Collaboration [1] participates in the heavy-ion (HI) programme which has been carried out at the LHC since 2010. Lead-lead (Pb+Pb) and proton-lead (p+Pb) collisions were provided at the centre-of-mass energies of 2.76 TeV, 5.02 TeV for Pb+Pb, and 5.02 TeV for p+Pb. In October 2017 a short period with xenon-xenon (Xe+Xe) collisions was taken. This opened up an opportunity of studying impact of different geometries on a broad range of observables. Moreover, the HI programme is supplemented with measurements in the pp system, which serve as a reference to disentangle initial- from final-state effects.

2. Electromagnetic interactions in the QGP

The strong electromagnetic field associated with highly boosted nuclei at the LHC can be utilised to study the scattering of the quasi-real photons emitted coherently from the nuclei as they pass by next to each other. These are so-called Ultra-Peripheral Collisions (UPC). In the previous measurements of exlusive production of di-muon pairs [2] and light-by-light scattering [3], ATLAS already demonstrated that photon

fluxes emerging from Pb beams are well modelled by the STARlight generator. Also in those measurements, an acoplanarity distribution ($\alpha = 1 - \frac{\Delta \phi}{\pi}$, where $\Delta \phi$ is a distance in azimuth between final-state particles) was measured and proved to be powerful in discriminating between signal and background processes.

Very recenty ATLAS has explored a potential of observing events from exclusive production of $\gamma\gamma \to \mu^+\mu^-$ contributing to a sample of inelastic minimum-bias Pb+Pb collisions [4]. After evaluating and removing the contribution from background sources, the azimuthal angle $(\Delta\phi)$ and transverse momentum (p_T) correlations between the muons are measured as a function of collision centrality.

Figure 1 shows the background-subtracted acoplanarity distribution in different centrality intervals. Each distribution is normalised to unity over its measured range. The > 80% distribution with a significant contribution from UPC events is plotted in each panel for comparison. A clear, centrality-dependent broadening is seen in the acoplanarity distributions when compared to the > 80% interval. The corresponding distribution from the $\gamma\gamma \to \mu^+\mu^-$ MC samples is also shown. The MC α distributions show almost no centrality dependence, indicating that the broadening evident in the data is notably larger than that expected from detector effects. One potential source of modification is the final-state interaction of the produced leptons with the electric charges in the QGP. Assuming that the broadening of the α distribution results from transfers of a small amount of p_T to each muon, in the 0–10% centrality interval that scale, assumed to be the RMS momentum transfer to each final-state muon in the transverse plane, is evaluated to amount to 70 ± 10 MeV.

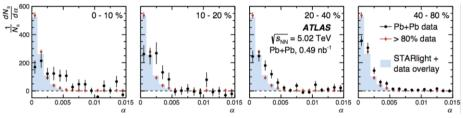


Fig. 1. Background-subtracted acoplanarity distribution (α) in four centrality intervals in Pb+Pb data [4]. A comparison to the STARlight calculation for $\gamma\gamma \to \mu^+\mu^-$ is also shown. The distributions are normalised to unity over their measured range.

3. Jet quenching

Using the large statistics of the 2015 Pb+Pb data, ATLAS finalised measurements of inclusive jet nuclear modification factor (R_{AA}) [5], as well as jet fragmentation functions [6]. Those results provide very detailed studies of inclusive jet production as a function of jet p_T , rapidity (y) and centrality in comparison to the reference pp data collected at 5.02 TeV.

The $R_{\rm AA}$ evaluated as a function of jet $p_{\rm T}$ for two centrality intervals 0–10% and 30–40% is presented in the left panel of Fig. 2. The $R_{\rm AA}$ value is obtained for jets with |y| < 2.1 and with $p_{\rm T}$ between 80–1000 GeV. A clear suppression of jet production in central Pb+Pb collisions relative to pp collisions is observed. In the 0-10% centrality interval, $R_{\rm AA}$ is approximately 0.45 at $p_{\rm T}=100$ GeV, and is observed to grow slowly (quenching decreases) with increasing jet $p_{\rm T}$, reaching a value of 0.6 for jets with $p_{\rm T}$ around 800 GeV. In the same figure, the $R_{\rm AA}$ values at 5.02 TeV are compared with the previous measurements at $\sqrt{s_{\rm NN}}=2.76$ TeV. The two measurements agree within their uncertainties in the overlapping $p_{\rm T}$ region. The apparent reduction of the size of systematic uncertainties in the new measurement is possible thans to large samples of pp and Pb+Pb data collected during the same LHC running period.

Further insight in jet quenching can be obtained by studying jet fragmentation functions. The right panel of Fig. 2 presents a ratio of transverse jet fragmentation functions $D(p_T)$ in Pb+Pb to those extracted in pp collisions as a function of jet fragment p_T for three jet p_T intervals. The $R_{D(p_T)}$ is above unity (enhancement) for low p_T jet fragments, drops below unity for intermediate jet p_T fragments (suppression) and becomes larger than unity again for jet fragment p_T around 50 GeV. There is no significant difference between $R_{D(p_T)}$ for three jet p_T intervals. A comparison between the data and the hybrid model calculation is also shown.

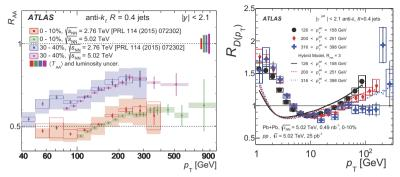


Fig. 2. (Left) Inclusive jet R_{AA} as a function of jet p_T for jets with |y| < 2.1 in 0–10% and 30–40% centrality intervals compared to the same quantity measured in 2.76 TeV Pb+Pb collisions [5]. (Right) $R_{D(p_T)}$ ratios for three jet p_T ranges: 126–158 GeV (circles), 200–251 GeV (diamonds) and 316–398 GeV (crosses) compared with calculations from the hybrid model with $R_{res} = 3$ [6].

The model is able to describe the intermediate- and high- p_T regions for jet fragments, while it fails in the low- p_T region.

The ATLAS Collaboration performed a preliminary measurement of the angular distribution of charged particles around the jet axis in 5.02 TeV Pb+Pb and pp data [7]. The measured yields are defined as:

$$R_{D(p_{\rm T})} = \frac{1}{N_{\rm iet}} \frac{1}{2\pi r} \frac{{\rm d}^2 n_{\rm ch}(r)}{{\rm d}r {\rm d}p_{\rm T}},$$
 (1)

where $N_{\rm jet}$ is the total number of jets, $2\pi r dr$ is the area of the annulus at a given distance r from the jet axis ($r=\sqrt{\Delta\eta^2+\Delta\phi^2}$ with $\Delta\eta$ and $\Delta\phi$ being the relative differences between the charged particle and the jet axis, in pseudorapidity and azimuth respectively), dr is the width of the annulus and $n_{\rm ch}(r)$ is the number of charged particles within a given annulus. Results are presented as a function of Pb+Pb collision centrality, and both jet and charged-particle $p_{\rm T}$ in the left panel of Fig. 3. Ratios of $D(p_{\rm T},r)$ distributions in Pb+Pb to those measured in $p_{\rm P}$ collisions as a function of r for six charged-particle $p_{\rm T}$ intervals spanning values between 1.6–63.1 GeV in 0–10% centrality, and for jet $p_{\rm T}$ between 200–251 GeV are shown. The $R_{D(p_{\rm T},r)}$ grows with increasing r for r < 0.3 and is approximately constant for 0.3 < r < 0.6. For $p_{\rm T} > 4.0$ GeV, $R_{D(p_{\rm T},r)}$ grows with increasing r for r < 0.3 and is approximately constant for 0.3 < r < 0.6. The observed behaviour inside the jet (r < 0.4) agrees with the measurement of the inclusive jet fragmentation functions [6], where yields of the low- $p_{\rm T}$ fragments are observed to be enhanced and yields of charged particles with intermediate $p_{\rm T}$ are suppressed. The measured dependence of $R_{D(p_{\rm T},r)}$ suggests that the energy lost by jets through the jet quenching process is being transferred to particles with $p_{\rm T} < 4.0$ GeV with larger radial distances.

ATLAS also measures inclusive jet mass (*m*) divided by the jet transverse momentum [8]. This fully-unfolded measurement of the jet structure is sensitive to the angular and momentum correlations of the jet constituents. These correlations can be used to study modifications of jets in HI collisions, where they provide complementary information to previously measured jet fragmentation functions.

The right panel of Fig. 3 presents R_{AA} as a function of m/p_T in 0–10% centrality for jet p_T between 126–158 GeV. For all centrality bins, these values have no significant dependence on m/p_T . They are also observed to be consistent with the inclusive jet R_{AA} .

A preliminary measurement of the balance between isolated photons and inclusive jets in p_T in 5.02 TeV Pb+Pb and p_P data is performed. Photons with $p_T^{\gamma} > 63.1$ GeV and $|\eta^{\gamma}| < 2.37$ are paired inclusively with all jets that have $p_T > 31.6$ GeV and $|\eta| < 2.8$ in the event. The transverse momentum balance given by the jet-to-photon p_T ratio, $x_{J\gamma}$, are measured for pairs with azimuthal opening angle $|\Delta \phi| > 7\pi/8$. Distributions of the per-photon jet yield $(1/N_{\gamma})(dN/dx_{J\gamma})$ are corrected for detector effects via a two-dimensional unfolding procedure and reported at the particle level for the first time.

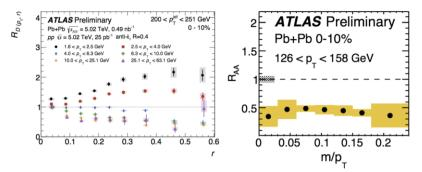


Fig. 3. (Left) Ratios of $D(p_T, r)$ distributions in 0–10% Pb+Pb collisions to pp collisions as a function of angular distance r for jet p_T of 200 to 251 GeV for six p_T selections [9]. (Right) Jet R_{AA} as a function of m/p_T in 0–10% centrality for jet p_T between 126–158 GeV [8].

Figure 4 shows the measured $x_{J\gamma}$ distribution in five centrality intervals of Pb+Pb collisions for $p_T^{\gamma} = 63.1 - 79.6$ GeV in comparison to the $x_{J\gamma}$ distribution from pp collisions. The $x_{J\gamma}$ distributions in Pb+Pb collisions evolve smoothly with centrality. For peripheral collisions with centrality 50–80%, they are similar to those measured in pp collisions. However, in increasingly more central collisions, the distributions become systematically more modified. The $x_{J\gamma}$ distribution in the most central 0–10% events is so strongly modified that it is monotonically decreasing over the measured $x_{J\gamma}$ range and no peak is observed.

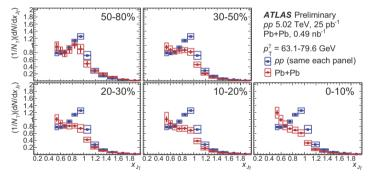


Fig. 4. Photon-jet p_T balance distributions $(1/N_\gamma)(dN/dx_{J\gamma})$ in pp events (blue, reproduced on all panels) and Pb+Pb events (red) with each panel denoting a different centrality selection [7].

To probe physics of jet quenching in HI collisions with nuclei lighter than Pb, the transverse momentum asymmetry of dijet pairs and production rates of charged particles are measured by ATLAS with Xe+Xe collisions collected in October 2017 [10]. Figure 5 presents charged-hadron $R_{\rm AA}$ as a function of $p_{\rm T}$ for three centrality and $\langle N_{\rm part} \rangle$ intervals along with the measurement from the Pb+Pb system. The $R_{\rm AA}$ is compared between Xe+Xe and Pb+Pb data at 5.02 TeV. Even though they have different centralities, the $\langle N_{\rm part} \rangle$ for the same $p_{\rm T}$ intervals are comparable. The Xe+Xe data shows more suppression than the Pb+Pb data in more central collisions, and less suppression in more peripheral collisions.

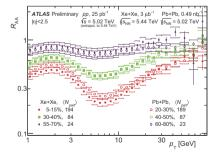


Fig. 5. Charged-hadron $R_{\rm AA}$ as a function of $p_{\rm T}$ measured in Xe+Xe collisions 5.44 TeV (closed markers) and in Pb+Pb collisions at 5.02 TeV (open markers) [10].

4. Quarkonia and heavy-flavour production

The ATLAS Collaboration finalised a detailed study on prompt and non-prompt J/ψ and $\psi(2S)$ production and suppression at high $p_{\rm T}$ in 5.02 TeV Pb+Pb and pp collisions [11]. The measurements of per-event yields, nuclear modification factors, and non-prompt fractions are performed in the di-muon decay channel for $9 < p_{\rm T}^{\mu\mu} < 40$ GeV in di-muon transverse momentum, and $2.0 < y_{\mu\mu} < 2.0$ in rapidity. Strong suppression is found in Pb+Pb collisions for both prompt and non-prompt J/ψ , as well as for prompt and non-prompt $\psi(2S)$, increasing with event centrality. The suppression of prompt $\psi(2S)$ is observed to be stronger than that of J/ψ , while the suppression of non-prompt $\psi(2S)$ is equal to that of the non-prompt J/ψ within uncertainties, consistent with the expectation that both arise from b-quarks propagating through the medium. Despite prompt and non-prompt J/ψ arising from different mechanisms, the dependence of their nuclear modification factors on centrality is found to be similar.

The left panel of Fig. 6 shows a p_T -dependence of the nuclear modification factor for prompt J/ψ mesons reconstructed via the muon channel at 5.02 TeV in the 0–20% centrality bin. The R_{AA} is at the level of 0.25 at $p_T = 9$ GeV and tends to increase slowly with p_T . The ATLAS measurement at high p_T nicely complements the ALICE results for $p_T < 12$ GeV that are also shown on the same figure.

Recently the ATLAS Collaboration also evaluated elliptic flow of J/ψ with respect to the event plane in 5.02 TeV Pb+Pb collisions and presented preliminary results as a function of transverse momentum, rapidity and centrality [12]. It is observed that prompt and non-prompt J/ψ mesons have non-zero elliptic flow. Prompt J/ψ v_2 decreases as a function of p_T , while non-prompt J/ψ v_2 is flat over the studied kinematical region. There is no dependence on rapidity or centrality observed. The right panel of Fig. 6 shows results for the v_2 as a function of p_T for prompt and non-prompt J/ψ as measured by ATLAS compared with inclusive J/ψ at $p_T < 12$ GeV, as measured by ALICE at 5.02 TeV, and prompt J/ψ at 6.5 < $p_T < 30$ GeV, by CMS at 2.76 TeV. Despite different rapidity selections, the ATLAS data is found to be in reasonable agreement with the ALICE and CMS data in the overlapping p_T region.

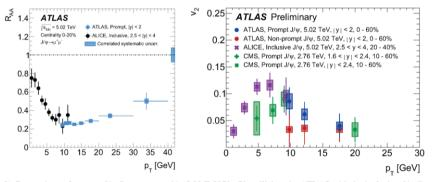


Fig. 6. (Left) Comparison of prompt J/ψ R_{AA} measured in 5.02 TeV Pb+Pb collisions by ATLAS with the inclusive J/ψ R_{AA} measured by ALICE [11]. (Right) v_2 as a function of p_T for prompt and non-prompt J/ψ as measured by ATLAS compared with inclusive J/ψ at $p_T < 12$ GeV, as measured by ALICE at 5.02 TeV, and prompt J/ψ at 6.5 $< p_T < 30$ GeV by CMS at 2.76 TeV [12].

The ATLAS Collaboration also finalised a measurement of the production of muons from heavy-flavour decays in 2.76 TeV Pb+Pb and pp collisions [13]. Results are provided in the muon transverse momentum range $4 < p_T < 14$ GeV and for five centrality intervals. Backgrounds arising from in-flight pion and kaon decays, hadronic showers, and mis-reconstructed muons are statistically removed using a template-fitting procedure. The heavy-flavor muon differential cross-sections and per-event yields are measured in pp and Pb+Pb collisions, respectively.

Figure 7 presents the heavy-flavour muon R_{AA} as a function of p_T . The R_{AA} does not depend on p_T within the uncertainties of the measurement. The R_{AA} decreases between peripheral 40–60% collisions, where it is about 0.65, to more central collisions, reaching a value of about 0.35 in the 0–10% centrality interval. In Ref. [13] the azimuthal modulation of the heavy-flavor muon yields is also measured and the

associated Fourier coefficients v_n for n=2, 3 and 4 are given as a function of p_T and centrality. They vary slowly with p_T and show a systematic variation with centrality which is characteristic of other anisotropy measurements, such as that observed for inclusive hadrons.

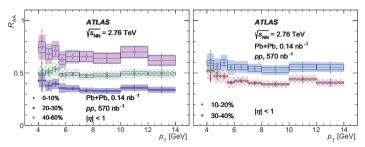


Fig. 7. Heavy-flavuor muon R_{AA} as a function of p_T for five centrality intervals in 2.76 TeV Pb+Pb collisions [13].

5. Collectivity in small and large systems

One active area of ongoing research is investigation of the nature of the long-range ridge observed in two-particle correlations in small collision systems such as pp and p+Pb. To understand the multi-particle nature of the long-range collective phenomenon in those systems, the ATLAS Collaboration performed a measurement of symmetric cumulants $\mathrm{sc}_{n,m}\{4\}$ and asymmetric cumulants $\mathrm{ac}_n\{3\}$ which probe four- and three-particle correlations of two flow harmonics ν_n and ν_m in 13 TeV pp, 5.02 TeV p+Pb, and 2.76 TeV peripheral Pb+Pb collisions [14]. The large non-flow background from dijet production present in the standard cumulant method is suppressed using a method of subevent cumulants.

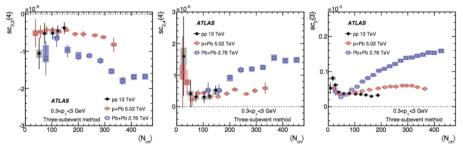


Fig. 8. The $\langle N_{ch} \rangle$ dependence of sc_{2.3}{4} (left), sc_{2.4}{4} (middle) and ac₂{3} (right) in 0.5 < p_T < 5 GeV obtained for pp collisions (solid circles), p+Pb collisions (open circles) and low-multiplicity Pb+Pb collisions (open squares) [14].

Figure 8 shows a comparison of cumulants for the three collision systems. The three panels present the results for $sc_{2,3}\{4\}$, $sc_{2,4}\{4\}$, and $ac_{2}\{3\}$ for charged particles with $0.3 < p_{T} < 3$ GeV. These results indicate a negative correlation between ν_{2} and ν_{3} and a positive correlation between ν_{2} and ν_{4} . Such correlation patterns have previously been observed in large collision systems, but are now confirmed also in the small collision systems, once non-flow effects are adequately removed in the measurements. In the multiplicity range covered by the pp collisions, $\langle N_{ch} \rangle < 150$, the results for symmetric cumulants $sc_{2,3}\{4\}$ and $sc_{2,4}\{4\}$ are comparable among the three systems. In the range $\langle N_{ch} \rangle > 150$, $|sc_{2,3}\{4\}|$ and $sc_{2,4}\{4\}$ are larger in Pb+Pb than in p+Pb collisions. The results for $ac_{2}\{3\}$ are similar among the three systems at $ac_{2,4}\{4\}$ are larger in Pb+Pb deviate from each other at higher $ac_{2,4}\{4\}$ are similar among the three systems at $ac_{2,4}\{4\}$ are slightly with $ac_{2,4}\{4\}$ are approximately constant or decrease slightly with $ac_{2,4}\{4\}$ and $ac_{2,4}\{4\}$ are similar increases as a function of $ac_{2,4}\{4\}$ are similarity between different collision systems and the weak dependence of these observables on the $ac_{2,4}\{4\}$ are similar input for understanding the space-time dynamics and the properties of the medium created in small collision systems.

Using a data set of Xe+Xe collisions collected at 5.44 TeV, ATLAS measured flow harmonics with the scalar method (SP) and correlation techniques involving 2, 4 and 6 particles [15]. Centrality and p_T -dependence of the v_n are studied. Figure 9 shows the v_n harmonics integrated over the $0.5 < p_T < 5 \text{ GeV}$ range. The values are compared to those obtained for Pb+Pb and are shown as a function of centrality. The small differences are related to differences in the initial-collision geometry and subtle differences due to the system size. Detailed studies of scaling of v_n and cumulants with $\langle N_{\text{part}} \rangle$ confirm the main source of v_2 to be the initial geometry, while geometry fluctuations to be the origin of differences for v_n with n > 2.

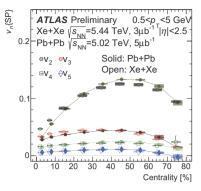


Fig. 9. The ν_n n=2-5 measured with the SP method in Xe+Xe and Pb+Pb collisions as a function of centrality percentile [15]. The Pb+Pb data points are shifted along the centrality axis, for clarity.

ATLAS also measured the modified Pearson's correlation coefficient to quantify correlations between flow coefficients and mean $p_{\rm T}$ of charged particles in the event using 5.02 TeV Pb+Pb data [16]. It can be used in further experimental studies to understand the underlying mechanism of QGP dynamics and constrain theoretical models attempting to describe them.

6. Summary

The ATLAS Collaboration presented many new results covering Pb+Pb, p+Pb, pp, and also data from the new Xe+Xe system collected for the first time at the LHC. These measurements provide new information on electromagnetic interactions, the jet quenching, quarkonia and heavy-flavour suppression, as well as comprehensive results which provide further insight into the collectivity phenomenon of small collision systems.

This work was supported in part by Polish National Science Centre grant DEC-2016/23/B/ST2/01409, by the AGH UST statutory tasks No. 11.11.220.01/4 within subsidy of the Ministry of Science and Higher Education, and by PL-Grid Infrastructure.

References

- [1] ATLAS Collaboration, JINST 3 (2008) S08003. doi:10.1088/1748-0221/3/08/S08003.
- [2] ATLAS Collaboration, http://cdsweb.cern.ch/record/2157689, ATLAS-CONF-2016-025.
- [3] ATLAS Collaboration, arXiv:1702.01625 [hep-ex], Nature Physics 13 (2017) 852.
- [4] ATLAS Collaboration, arXiv:1806.08708 [nucl-ex], submitted to PRL.
- [5] ATLAS Collaboration, arXiv:1805.05635 [nucl-ex], submitted to PLB.
- [6] ATLAS Collaboration, arXiv:1805.05424 [nucl-ex], submitted to PRC.
- [7] ATLAS Collaboration, http://cdsweb.cern.ch/record/2318869, ATLAS-CONF-2018-010.
- [8] ATLAS Collaboration, http://cdsweb.cern.ch/record/2319867, ATLAS-CONF-2018-014.
- [9] ATLAS Collaboration, http://cdsweb.cern.ch/record/2318868, ATLAS-CONF-2018-009.
- [10] ATLAS Collaboration, http://cdsweb.cern.ch/record/2318588, ATLAS-CONF-2018-007.
- [11] ATLAS Collaboration, arXiv:1805.04077 [nucl-ex], submitted to EPJC.
- [12] ATLAS Collaboration, http://cdsweb.cern.ch/record/2319788, ATLAS-CONF-2018-013.
- [13] ATLAS Collaboration, arXiv:1805.05220 [nucl-ex], submitted to PRC.
- [14] ATLAS Collaboration, arXiv:1807.02012 [nucl-ex], submitted to PLB.
- [15] ATLAS Collaboration, http://cdsweb.cern.ch/record/2318870, ATLAS-CONF-2018-011.
- [16] ATLAS Collaboration, http://cdsweb.cern.ch/record/2318589, ATLAS-CONF-2018-008.